Does black hole continuum spectrum signal $f(R)$ gravity in higher dimensions?

Indrani Banerjee,[*] Bhaswati Mandal,[†] and Soumitra SenGupta[‡]
School of Physical Sciences, Indian Association for the Cultivation of Science, Kolkata-700032, India

(Received 1 August 2019; published 3 January 2020)

Extra dimensions, which led to the foundation and inception of string theory, provide an elegant approach to force unification. With bulk curvature as high as the Planck scale, higher curvature terms, namely, $f(R)$ gravity, seem to be a natural addendum in the bulk action. These can not only pass the classic tests of general relativity but also serve as potential alternatives to dark matter and dark energy. With interesting implications in inflationary cosmology, gravitational waves, and particle phenomenology, it is worth exploring the impact of extra dimensions and $f(R)$ gravity in black hole accretion. Various classes of black hole solutions have been derived that bear nontrivial imprints of these ultraviolet corrections to general relativity. This, in turn, gets engraved in the continuum spectrum emitted by the accretion disk around black holes. Since the near horizon regime of supermassive black holes manifest maximum curvature effects, we compare the theoretical estimates of disk luminosity with quasar optical data to discern the effect of the modified background on the spectrum. In particular, we explore a certain class of black hole solution bearing a striking resemblance to the well-known Reissner-Nordström–de Sitter/anti–de Sitter/flat spacetime, which, unlike general relativity, can also accommodate a negative charge parameter. By computing error estimators like chi square, Nash-Sutcliffe efficiency, index of agreement, etc., we infer that optical observations of quasars favor a *negative* charge parameter, which can be a possible indicator of extra dimensions. The analysis also supports an asymptotically de Sitter spacetime with an estimate of the magnitude of the cosmological constant whose origin is solely attributed to $f(R)$ gravity in higher dimensions.

DOI: 10.1103/PhysRevD.101.024013

I. INTRODUCTION

General relativity (GR) is a classic example of a scientific theory that is elegant, simple, and powerful. To date, it is the most successful theory of gravity in explaining a plethora of observations, namely, the perihelion precession of mercury, bending of light, and gravitational redshift of radiation from distant stars, to name a few [1–3]. Very recently, the shadow of the black hole in M87 observed by the Event Horizon Telescope has further added to its phenomenal success [4–6]. Yet it is instructive to subject GR to further tests since it is marred with unresolved issues like singularities [7–9] and falls short in explaining the nature of dark energy and dark matter [10–14]. Moreover, the quantum nature of gravity is still elusive and ill understood [15–17]. All this makes the quest for a more complete theory of gravity increasingly compelling such that it yields GR in the low energy limit. Consequently, a surfeit of alternate gravity models have been proposed that can potentially fulfill the deficiencies in GR. A viable alternate gravity theory must be free from ghost modes, be consistent with solar-system-based tests, should not engender a fifth force in local physics, and should successfully explain observations that GR fails to address. The alternate gravity models that fulfill these benchmarks can be broadly classified into three categories: (i) modified gravity models where the gravity action is supplemented with higher curvature terms, e.g., $f(R)$ gravity [18–21], Lanczos-Lovelock models, etc. [22–26], (ii) extra-dimensional models that alter the effective four-dimensional gravitational field equations due to the bulk Weyl stresses and higher order corrections to the stress tensor [27–33], and (iii) scalar-tensor theories of gravity, which include the Brans-Dicke theory and the more general Horndeski models [34–37].

In this work, we will consider modifications to the gravity sector by introducing $f(R)$ gravity in five dimensions. Among the various modified gravity models, $f(R)$ theories have attracted the attention of physicists for a long time [18,38–40] since they invoke the simplest modification to the Einstein-Hilbert action and yet exhibit sufficient potential to address a host of cosmological and astrophysical observations. These include, but are not limited to, the late-time acceleration [41,42] and the initial power-law

[*]tpib@iacs.res.in
[†]tpbm3@iacs.res.in
[‡]tpssg@iacs.res.in

inflation of the Universe [43], the four cosmological phases [19,44], the rotation curves of spiral galaxies [45,46], and the detection of gravitational waves [47–49]. Although these models are plagued with ghost modes, certain $f(R)$ models, e.g., $f(R)$ theory on a constant curvature hypersurface, can be shown to be ghost free [50–52]. In addition, they can successfully surpass the Solar System tests that only impose constraints on $f''(R)$ and hence on the model parameters [53–55].

Extra dimensions, on the other hand, were mainly invoked to provide a framework to unify gravity and electromagnetism [56–58]. This subsequently provided a framework for string theory and M theory that succeeded in unifying all the known forces under a single umbrella [59–61]. The large radiative corrections to the Higgs mass arising due to the huge disparity between the electroweak scale and the Planck scale [62–66] led to the emergence of a diversity of string inspired brane world models. Most of these models assume that the observable Universe is confined in a 3-brane where all the Standard Model particles and fields reside while gravity permeates to the bulk [62–68]. They possess interesting phenomenological implications [69–74] and distinct observational signatures, including production of miniature black holes which can be tested in present and future collider experiments [75,76]. On the galactic scale, they offer an alternative to the elusive dark matter [45,77–80], while in cosmology they have interesting implications in the inflationary epoch [81–87] and also serve as a possible proxy to dark energy [31,88–93]. Since the ultraviolet nature of gravity is unknown, it is often believed that, in the high energy regime, the deviations from Einstein gravity may manifest through the existence of extra dimensions. Moreover, the bulk curvature is expected to be as high as the Planck scale and hence higher order corrections to the gravity action should become relevant in the high energy regime.

In this work, we consider a single brane world scenario with a positive tension that is embedded in a five-dimensional bulk containing $f(R)$ gravity. The addition of $f(R)$ gravity in higher dimensions causes substantial modification to the effective gravitational field equations on the brane [27,30,33,94,95], which are obtained from the Gauss-Codazzi equation and the junction conditions [96]. Such deviations from Einstein's equations are expected to become more conspicuous in the high energy and high curvature domain. Therefore, the near horizon regime of black holes, where the curvature effects are maximum, seems to be an ideal astrophysical laboratory to test these models against observations.

Various classes of vacuum solutions of these field equations have been obtained [28,29,32,97,98], which possess distinct signatures of extra dimensions and $f(R)$ gravity. In the event the vacuum solutions are static and spherically symmetric, the electric part of the Weyl tensor can be decomposed into terms involving "dark radiation" and "dark pressure." Suitable integrability conditions lead to different classes of vacuum solutions, which determine the spacetime geometry. The solutions thus derived exhibit substantial modification from the well-known Schwarzschild spacetime, which are attributed to the nonlocal effects of the bulk Weyl tensor and $f(R)$ gravity in the action. These deviations in the background spacetime are sculpted in the continuum spectrum emitted from the accretion disk around black holes. In particular, since the curvature effects are maximum in supermassive black holes, the quasar continuum spectra can act as potential astrophysical probes to establish, falsify, or constrain these models.

In a recent work [99], we explored an exact black hole solution in the brane with bulk Einstein gravity. It resembles the well-known Reissner-Nordström spacetime in general relativitywhere the tidal charge parameter can assume both signatures. By comparing the disk luminosity of quasars in such a background with the corresponding observations, we conclude that a negative charge parameter is favored, which is characteristic of brane world black holes. Adding $f(R)$ gravity in the bulk action adds a vacuum energy term to the aforesaid black hole solution, where the cosmological constant owes its origin to terms involving $f(R)$ gravity in higher dimensions. In this work, we investigate the effect of such a spacetime on the quasar continuum spectrum, which enables us to explore the signature of the tidal charge parameter in the presence of the cosmological constant term in the metric. Subsequently, we also derive constraints on the magnitude of the cosmological constant from quasar optical data. Further, we also investigate the effect of other black hole solutions on the quasar continuum spectrum, which are derived by altering the relations connecting the dark radiation and dark pressure.

The paper is organized as follows: In Sec. II, we discuss the modifications induced in the gravitational field equations due to the presence of bulk $f(R)$ gravity. The static, spherically symmetric, vacuum solutions of these field equations are reviewed in Sec. III. In Sec. IV, we examine the properties of the black hole continuum spectrum in presence of the background spacetimes discussed in Sec. III. Section V is dedicated to numerical analysis where the theoretically computed luminosities from the accretion disk of 80 quasars are compared with the corresponding observed values. Finally, we conclude with a summary and discussion of our results in Sec. VI.

Throughout this paper, the Greek indices denote the four-dimensional spacetime and capitalized Latin letters represent the five-dimensional bulk indices. We work in geometrized units with $G = 1 = c$ and the metric convention is mostly positive.

II. STATIC, SPHERICALLY SYMMETRIC BLACK HOLE SOLUTIONS IN HIGHER DIMENSIONAL $f(\mathcal{R})$ GRAVITY

In this section, we consider $f(R)$ gravity in the bulk action and derive the effective gravitational field equations on the brane. The bulk action $\mathcal{A}$ assumes the form

$$\mathcal{A} = \int d^5x\sqrt{-G}\left[\frac{f(R)}{2\kappa_5^2} + \mathcal{L}_m\right], \tag{1}$$

where G_{AB} is the bulk metric, R is the bulk Ricci scalar, and $\mathcal{L}_m$ is the matter Lagrangian. The bulk indices are denoted by capitalized Latin letters, e.g., A, B, which run over all spacetime dimensions, while Greek letters denote the brane coordinates. The gravitational field equation obtained by varying the bulk action with respect to G_{AB} is given by

$$f'(R)R_{AB} - \frac{1}{2}G_{AB}f(R) + G_{AB}\Box f'(R) - \nabla_A\nabla_B f'(R) = \kappa_5^2 T_{AB}, \tag{2}$$

where R_{AB} is the bulk Ricci tensor, $\kappa_5^2 = 8\pi G_5$ is the five-dimensional gravitational constant, and the prime denotes the derivative with respect to R. The bulk energy-momentum tensor can be written as

$$T_{AB} = -\Lambda_5 G_{AB} + \delta(\phi)(-\lambda_T g_{\mu\nu} + \tau_{\mu\nu})e_A^\mu e_B^\nu, \tag{3}$$

where Λ_5, the negative vacuum energy density on the bulk, the brane tension λ_T, and the brane energy-momentum tensor $\tau_{\mu\nu}$ are the sources of the gravitational field on the bulk. The various physical quantities on the bulk are projected onto the brane with the help of the projector e_A^μ. The brane is located at $\phi = 0$ (where ϕ represents the extra coordinate) and the induced metric on the $\phi = 0$ hypersurface is represented by $g_{\mu\nu}$.

In order to obtain the effective gravitational field equations on the brane, the Gauss-Codazzi equation is used, which connects the bulk Riemann tensor to that of the brane with the help of the projector e_A^μ and the extrinsic curvature tensor $K_{\mu\nu}$. The extrinsic curvature is related to the covariant derivative of the normalized normals to the brane n^A and encodes the embedding of the brane into the bulk. The presence of a brane energy-momentum tensor leads to a discontinuity in $K_{\mu\nu}$ across the brane. Israel junction conditions and a Z_2 orbifold symmetry relates this discontinuity in the extrinsic curvature to the brane energy-momentum tensor. For a detailed derivation, one is referred to [29,32,33,96].

With the above considerations, the effective four-dimensional gravitational field equations on the brane assume the form

$$\mathcal{R}_{\mu\nu} - \frac{1}{2}\mathcal{R}g_{\mu\nu} = -\Lambda_4 g_{\mu\nu} + 8\pi G_4\tau_{\mu\nu} + \kappa_5^4\pi_{\mu\nu} + Q_{\mu\nu} - E_{\mu\nu}, \tag{4}$$

where

$$\Lambda_4 = \frac{1}{2}\kappa_5^2\left[\frac{\Lambda_5}{f'(R)} + \frac{1}{6}\kappa_5^2\lambda_T^2\right], \tag{5}$$

$$G_4 = \frac{\kappa_5^4\lambda_T}{48\pi}, \tag{6}$$

$$\pi_{\mu\nu} = -\frac{1}{4}\tau_{\mu\alpha}\tau_\nu^\alpha + \frac{1}{12}\tau\tau_{\mu\nu} + \frac{1}{8}g_{\mu\nu}\tau_{\alpha\beta}\tau^{\alpha\beta} - \frac{1}{24}g_{\mu\nu}\tau^2, \tag{7}$$

$$Q_{\mu\nu} = \left[h(R)g_{\mu\nu} + \frac{2}{3}\frac{\nabla_A\nabla_B f'(R)}{f'(R)}(e_\mu^A e_\nu^B + n^A n^B g_{\mu\nu})\right]_{\phi=0}, \tag{8}$$

$$h(R) = \frac{1}{4}\frac{f(R)}{f'(R)} - \frac{1}{4}R - \frac{2}{3}\frac{\Box f'(R)}{f'(R)}, \tag{9}$$

$$E_{\mu\nu} = C_{ABCD}e_\mu^A n^B e_\nu^C n^D, \tag{10}$$

$$\tag{11}$$

In Eq. (4), $\mathcal{R}_{\mu\nu}$ and $\mathcal{R}$ refer to the Ricci tensor and Ricci scalar on the brane, while Λ_4 and G_4 represent the four-dimensional cosmological constant and gravitational constant, respectively. Equation (5) serves as the fine balancing relation of the Randall-Sundrum single brane model [27,67], which enables the brane tension to be tuned appropriately with the bulk cosmological constant to yield de Sitter, anti–de Sitter, or flat branes. In Eq. (4), $\pi_{\mu\nu}$ represents higher order terms associated with the brane energy-momentum tensor due to the local effects of the bulk on the brane. The term $Q_{\mu\nu}$ arises because of the presence of higher curvature terms in the bulk action. In the event $f(R) = R$, $Q_{\mu\nu} = 0$ and we recover the projected field equations on the brane due to pure Einstein gravity in the bulk. The expression for $Q_{\mu\nu}$ can be simplified further by assuming that $\partial_\mu R = 0$ when the second term in Eq. (8) vanishes (see, for example, [32]) such that

$$Q_{\mu\nu} = \left[h(R)g_{\mu\nu} + \frac{2}{3}\frac{\nabla_A\nabla_B f'(R)}{f'(R)}n^A n^B g_{\mu\nu}\right]_{\phi=0} = \mathcal{F}(R)g_{\mu\nu}. \tag{12}$$

Since the bulk Ricci scalar is expected to be a well-behaved quantity, it can be expanded in a Taylor series around $\phi = 0$, i.e.,

$$R = R_0 + R_1\phi + R_2\frac{\phi^2}{2} + \mathcal{O}(\phi^3), \tag{13}$$

where the coefficients are constants since R is independent of the brane coordinates. This implies that the derivatives of R evaluated at $\phi = 0$ in Eq. (12) will result in a constant contribution independent of the brane coordinates.

The last term on the right-hand side of Eq. (4) is $E_{\mu\nu}$, which epitomizes the electric part of the bulk Weyl tensor with its origin in the nonlocal effect from the free bulk gravitational field. It is the transmitted projection of the bulk Weyl tensor C_{ABCD} on the brane, such that $E_{AC} = C_{ABCD}n^B n^D$ with the property $E_{\mu\nu} = E_{AB}e^A_\mu e^B_\nu$. The conservation of the matter energy-momentum tensor on the brane, i.e., $D_\nu\tau^\nu_\mu = 0$ (where D_ν represents the brane covariant derivative), leads to the constraint $D_\nu E^\nu_\mu - \kappa_5^4 D_\nu \pi^\nu_\mu = 0$, since $D_\nu \mathcal{F}(R)\delta^\nu_\mu = 0$ as the bulk Ricci scalar depends only on ϕ.

The symmetry properties of $E_{\mu\nu}$ allows an irreducible decomposition of the tensor in terms of a given four-velocity field u^μ [29,100],

$$E_{\mu\nu} = -k^4\left[U(r)\left(u_\mu u_\nu + \frac{1}{3}\zeta_{\mu\nu}\right) + 2Q_{(\mu}u_{\nu)} + P_{\mu\nu}\right], \tag{14}$$

where $k = \frac{\kappa_5}{\kappa_4}$ with $\kappa_4^2 = 8\pi G_4$, and $\zeta_{\mu\nu} = g_{\mu\nu} + u_\mu u_\nu$ is the projector orthogonal to u^μ. Note that $\kappa_4^2 = \kappa_5^4\lambda_T/6$, such that we retrieve general relativity in the limit $\lambda_T^{-1} \to 0$ [29]. In Eq. (14), the scalar $U(r) = -\frac{1}{k^4}E_{\mu\nu}u^\mu u^\nu$ is often known as the dark radiation term. The second term on the right-hand side of Eq. (14) consists of a spatial vector $Q_\mu = \frac{1}{k^4}\zeta^\alpha_\mu E_{\alpha\beta}u^\beta$, whereas the third term consists of a spatial, trace-free, symmetric tensor $P_{\mu\nu} = -\frac{1}{k^4}[\zeta^\alpha_{(\mu}\zeta^\beta_{\nu)} - \frac{1}{3}\zeta_{\mu\nu}\zeta^{\alpha\beta}]E_{\alpha\beta}$.

In order to obtain vacuum solutions on the brane, the brane should be source free such that $\tau_{\mu\nu} = \pi_{\mu\nu} = 0$. Thus, the gravitational field equations on the brane reduce to

$$\mathcal{R}_{\mu\nu} - \frac{1}{2}\mathcal{R}g_{\mu\nu} = -\Lambda_4 g_{\mu\nu} + \mathcal{F}(R)g_{\mu\nu} - E_{\mu\nu}. \tag{15}$$

In such a scenario, the effective four-dimensional cosmological constant is given by $\tilde{\Lambda} = \Lambda_4 - \mathcal{F}(\mathcal{R})$, while the conservation of the energy-momentum tensor on the brane simplifies to $D_\nu E^\nu_\mu = 0$. Additionally, if the solutions are static, the term Q_μ in Eq. (14) should vanish such that the conservation of brane energy-momentum tensor leads to

$$\frac{1}{3}\bar{D}_\mu U + \frac{4}{3}UA_\mu + \bar{D}^\nu P_{\nu\mu} + A^\nu P_{\nu\mu} = 0, \tag{16}$$

where $A_\mu = u^\nu D_\nu u_\mu$ is the four acceleration and $\bar{D}$ denotes the covariant derivative on the spacelike hypersurface orthonormal to u_μ. Further, if the solutions are spherically symmetric, we may write $A_\mu = A(r)r_\mu$, while the term $P_{\mu\nu}$ can be written as

$$P_{\mu\nu} = P(r)\left(r_\mu r_\nu - \frac{1}{3}\zeta_{\mu\nu}\right), \tag{17}$$

where $A(r)$ and $P(r)$ (also known as the dark pressure) are scalar functions of the radial coordinate r and r_μ is the unit radial vector.

In order to derive static, spherically symmetric solutions of Eq. (15), we consider a metric ansatz of the form

$$ds^2 = -e^{\nu(r)}dt^2 + e^{\lambda(r)}dr^2 + r^2(d\theta^2 + \sin^2\theta d\phi^2) \tag{18}$$

and solve for $\nu(r)$, $\lambda(r)$, $U(r)$, and $P(r)$, since Eq. (18) satisfies Eqs. (15) and (16). One can show that the solution of these equations leads to the following form for $e^{-\lambda}$ [32]:

$$e^{-\lambda} = 1 - \frac{\Lambda_4 - \mathcal{F}(R)}{3}r^2 - \frac{Q(r)}{r} - \frac{C}{r}, \tag{19}$$

where C is an arbitrary integration constant and $Q(r)$ is defined as

$$Q(r) = \frac{3}{4\pi G_4\lambda_T}\int r^2 U(r)dr. \tag{20}$$

From the form of $e^{-\lambda}$ it can be inferred that $Q(r)$ is the gravitational mass originating from the dark radiation and can be interpreted as the "dark mass" term. It is important to emphasize that, in the limit $f(R) \to R$, $\Lambda_4 \to 0$, and $U \to 0$, we get back the standard Schwarzschild solution and the constant of integration can then be identified with $C = 2G_4M$, where M is the mass of the gravitating body.

Further, one can show that, for a static, spherically symmetric spacetime, the ordinary differential equations for dark radiation $U(r)$ and dark pressure $P(r)$ satisfy [32]

$$\frac{dU}{dr} = -2\frac{dP}{dr} - 6\frac{P}{r} - \frac{(2U+P)[2G_4M + Q + \{\alpha(U+2P) + 2\chi/3\}r^3]}{r^2(1 - \frac{2G_4M}{r} - \frac{Q(r)}{r} - \frac{\Lambda_4 - \mathcal{F}(R)}{3}r^2)} \tag{21}$$

and

$$\frac{dQ}{dr} = 3\alpha r^2 U, \tag{22}$$

where $\alpha = \frac{1}{4\pi G_4\lambda_T}$ and $\chi = -\tilde{\Lambda} = \mathcal{F}(R) - \Lambda_4$. Equations (21) and (22) can be recast into a more convenient form, namely,

$$\frac{d\mu}{d\theta} = -(2\mu + p)\frac{\tilde{q} + \frac{1}{3}(\mu + 2p) + \frac{l}{3}}{1 - \tilde{q} + \frac{l}{6}} - 2\frac{dp}{d\theta} + 2\mu - 2p, \tag{23}$$

$$\frac{d\tilde{q}}{d\theta} = \mu - \tilde{q}, \tag{24}$$

by defining the variables

$$\tilde{q} = \frac{2G_4M + Q}{r}, \qquad \mu = 3\alpha r^2 U,$$
$$p = 3\alpha r^2 P, \qquad \theta = ln\, r, \qquad 2\chi r^2 = l. \tag{25}$$

Equations (23) and (24) can be referred to as the differential equations governing the source terms on the brane. For a detailed derivation of the differential equations for the metric components and the source terms, one is referred to [29,32]. In the next section, we shall review various static, spherically symmetric and vacuum solutions of Eq. (15) on the brane.

III. VARIOUS CLASSES OF SOLUTIONS ON THE BRANE

The source equations (23) and (24) for dark radiation and dark pressure cannot be solved simultaneously until we impose some further conditions on them. Hence, we choose some specific relations between dark radiation U and dark pressure P, necessarily defining the various equations of state in the framework of the brane world model. We will note that the different choices of equations of state will lead to very distinct solutions.

A. Case A: $P = 0$

This is the vanishing dark pressure case. The dark radiation and the dark mass can be evaluated by solving the coupled equations (23) and (24). With $P = 0$, these two equations simplify to

$$\frac{d\tilde{q}}{d\theta} = \mu - \tilde{q}, \tag{26}$$

$$\frac{d\mu}{d\theta} = 2\mu\left[\frac{6 - l - 2\mu - 12\tilde{q}}{6 + l - 6\tilde{q}}\right], \tag{27}$$

respectively. The above two equations can be combined to produce a single differential equation given by

$$(6 + l - 6\tilde{q})\frac{d^2\tilde{q}}{d\theta^2} + (26\tilde{q} - 6 + 3l)\frac{d\tilde{q}}{d\theta} + 4\left(\frac{d\tilde{q}}{d\theta}\right)^2 + 2\tilde{q}(14\tilde{q} - 6 + l) = 0. \tag{28}$$

Since l is not a constant in Eq. (28) we apply some approximate methods to find a solution for $\tilde{q}(\theta)$. By taking the Laplace transformation of Eq. (28) and using the convolution theorem, we get an integral solution for $\tilde{q}(\theta)$,

$$\tilde{q}(\theta) = \tilde{q}_0(\theta) + \int_{\theta_0}^{\theta} g(\theta - x)\left[3\tilde{q}\frac{d^2\tilde{q}}{dx^2} - 13\tilde{q}\frac{d\tilde{q}}{dx} - 2\left(\frac{d\tilde{q}}{dx}\right)^2 - 14\tilde{q}^2 - \chi e^{2x}\frac{d^2\tilde{q}}{dx^2} - 3\chi e^{2x}\frac{d\tilde{q}}{dx} - 2\chi e^{2x}\tilde{q}\right]dx \tag{29}$$

with the associated functions

$$g(\theta - x) = \frac{1}{9}[e^{2(\theta - x)} - e^{-(\theta - x)}], \tag{30}$$

$$\tilde{q}_0(\theta) = B_1 e^{-\theta} + B_2 e^{2\theta}, \tag{31}$$

$$B_1 = [3\tilde{q}(\theta_0) - \mu(\theta_0)]\frac{e^{\theta_0}}{3} = M_0 - \alpha U(r_0) r_0^3, \tag{32}$$

$$B_2 = \mu(\theta_0)\frac{e^{-2\theta_0}}{3} = \alpha U(r_0), \tag{33}$$

where $\theta_0 = ln\, r_0$ is an arbitrary point that can be associated with the vacuum boundary of a compact astrophysical object [29,32] and $M_0 = 2G_4M + Q(r_0)$.

Equation (29) can be solved by applying successive approximation methods. The zeroth-order solution denoted by $\tilde{q}_0$ is derived by considering only the linear part of Eq. (28). The full solution can thus be expressed as $\tilde{q}(\theta) = \lim_{m\to\infty}\tilde{q}_m(\theta)$ ($m \in N$ being the order of the equation) such that the iterative solution at mth order is connected to the $(m-1)$th order by the following differential equation [29,32]:

$$\tilde{q}_m(\theta) = \int_{\theta_0}^{\theta} H(\theta - x)\left[3\tilde{q}_{m-1}\frac{d^2\tilde{q}_{m-1}}{dx^2} - 13\tilde{q}_{m-1}\frac{d\tilde{q}_{m-1}}{dx} - 2\left(\frac{d\tilde{q}_{m-1}}{dx}\right)^2 - 14\tilde{q}_{m-1}^2 - \chi e^{2x}\frac{d^2\tilde{q}_{m-1}}{dx^2} - 3\chi e^{2x}\frac{d\tilde{q}_{m-1}}{dx} - 2\chi e^{2x}\tilde{q}_{m-1}\right]dx + \tilde{q}_{m-1}(\theta). \tag{34}$$

Once we determine the solution for $\tilde{q}(\theta)$ we can derive the solution for the metric components by using the gravitational field equations on the brane and the condition for the conservation of energy-momentum tensor. In the zeroth order, the static and spherically symmetric solution to the field equations is given by [29,32]

$$U = \frac{B_2}{\alpha}, \tag{35}$$

$$e^{\nu} = C_0\sqrt{\frac{\alpha}{B_2}}, \tag{36}$$

$$e^{-\lambda} = 1 - \frac{B_1}{r} - B_2 r^2, \tag{37}$$

where C_0 is an arbitrary constant of integration. Since α is positive, Eq. (36) implies that B_2 and, consequently, $U(r_0)$ should be positive. Also, the g_{tt} component of the metric should be positive, which implies $C_0 > 0$.

Iterating once more, we get the approximate expressions for $U(r)$ and $e^{\nu(r)}$ up to first order,

$$U = e^{-2\nu(r)}, \tag{38}$$

$$e^{\nu(r)} = C_0\sqrt{\frac{\alpha}{B_2}} + \sqrt{\frac{\alpha r_0}{2}}\sqrt{\frac{r}{B_2(r_0-r)[B_1 + B_2 r r_0^2 + B_2 r_0 r^2] + \frac{1}{3}B_2\chi r r_0(r_0^2 - r^2)}}. \tag{39}$$

Since we are interested in the distances much smaller compared to the cosmological horizon r_0, it is reasonable to assume $r \ll r_0$. Under this assumption, Eq. (39) simplifies considerably,

$$e^{\nu(r)} \simeq C_0\sqrt{\frac{\alpha}{B_2}} + \sqrt{\frac{\alpha}{2B_1B_2}}\rho^{-1/2}\left[1 + \frac{1}{\rho r}\right]^{-1/2}, \tag{40}$$

where $\rho = \frac{r_0^2}{B_1}(B_2 + \frac{\chi}{3})$. It is evident from Eq. (40) that $B_2 + \frac{\chi}{3}$ should be positive, while B_1 can assume both signatures. Further, if $r > 1/\rho$ we can perform a binomial expansion of Eq. (40), giving rise to a solution of the form

$$e^{\nu(r)} \simeq \delta + \beta - \frac{\beta}{2\rho r}, \tag{41}$$

where $\delta = C_0\sqrt{\frac{\alpha}{B_2}}$ and $\beta = \frac{1}{r_0}\sqrt{\frac{\alpha}{2B_2^2 + \frac{2B_2\chi}{3}}}$. Note that the dependence on $f(\mathcal{R})$ gravity comes from the parameter χ. Equation (41) can be rescaled such that the g_{tt} component of the metric assumes the form

$$e^{\nu(r)} \simeq 1 - \frac{r_1}{2r}\frac{1}{C_0 r_0(2B_2 + \frac{2\chi}{3})^{1/2} + 1} \simeq 1 - \frac{2G_4\tilde{M}}{r}, \tag{42}$$

where

$$r_1 = \frac{1}{\rho} = \frac{M_0 - \alpha U(r_0) r_0^3}{r_0^2(\alpha U(r_0) + \chi/3)}. \tag{43}$$

Therefore, it is clear from Eq. (42) that, in the regime $r_1 \ll r \ll r_0$, the g_{tt} component of the approximate metric is very similar to the Schwarzschild spacetime in general relativity, although the ADM mass $\tilde{M}$ has contributions from the inertial mass M as well as the higher curvature and higher dimension terms. The g_{tt} component solely determines the photon sphere r_{ph} and the radius of the marginally stable circular orbit r_{ms} of massive test particles. The photon sphere r_{ph} is obtained from the solution of

$$2g_{tt} - r g_{tt,r} = 0, \tag{44}$$

while the marginally stable circular orbit r_{ms} is evaluated from the solution of

$$r g_{tt} g_{tt,rr} = 2r g_{tt,r}^2 - 3 g_{tt} g_{tt,r}. \tag{45}$$

Note that $\tilde{M}$ should be positive, otherwise r_{ph} and r_{ms} become negative, which is unphysical. Since $\tilde{M}$ and C_0 are both positive, together they ensure that $B_1 > 0$.

In order to simplify our calculations, we scale the radial distance r in units of the gravitational radius $r_g = G_4\tilde{M}/c^2$, such that Eq. (42) assumes the form

$$e^{\nu(r)} \simeq 1 - \frac{2}{\tilde{r}}, \tag{46}$$

where $\tilde{r} = r/r_g = r/\tilde{M}$ (with $G_4 = c = 1$). The deviation of the approximate metric from the Schwarzschild spacetime is manifested in the g_{rr} term, where

$$g^{rr} = e^{-\lambda(r)} \simeq 1 - \frac{\tilde{\varepsilon}}{\tilde{r}} - 3\tilde{\gamma}\,\tilde{r} + \tilde{\eta}\tilde{r}^2 + \tilde{\sigma}\tilde{r}^4, \tag{47}$$

where

$$\tilde{\varepsilon} = \frac{\varepsilon}{r_g} = \frac{1}{r_g}\left\{\left[M_0 - \frac{\alpha U(r_0) r_0^3}{5}\right][1 - \alpha U(r_0) r_0^2] - \frac{4}{5}\alpha U(r_0) r_0^3\left[1 + \frac{\chi r_0^2}{3}\right]\right\},$$

$$\tilde{\gamma} = \gamma r_g = B_1 B_2 r_g,$$

$$\tilde{\eta} = \eta r_g^2 = r_g^2\left\{\left[B_2 + \frac{\chi}{3}\right][1 - 2B_2 r_0^2] - 2B_2\left[1 - \frac{B_1}{r_0}\right]\right\},$$

$$\tilde{\sigma} = \sigma r_g^4 = r_g^4\frac{6B_2}{5}\left(B_2 + \frac{\chi}{3}\right).$$

Since we are interested in black hole solutions, the curvature singularity at $r = 0$ must be covered by an event horizon. The radius of the event horizon $r_{\rm EH}$ is obtained from the real positive solutions of $e^{-\lambda(r)} = 0$. Since $g^{rr} = 0$ is a fifth-order algebraic equation, it always has at least one real root. For the real root to be positive, we need to choose the values of $\tilde{\varepsilon}$, $\tilde{\gamma}$, $\tilde{\eta}$, and $\tilde{\sigma}$ judiciously. From the previous discussion, it is evident that $\tilde{\gamma}$ and $\tilde{\sigma}$ are always positive, while $\tilde{\varepsilon}$ and $\tilde{\eta}$ can assume any signature. Further constraints on the values of $\tilde{\varepsilon}$, $\tilde{\gamma}$, $\tilde{\eta}$, and $\tilde{\sigma}$ are established from the fact that $r_{\rm EH} < r_{ph} < r_{ms}$.

The disadvantage of this choice of equation of state is that the metric does not represent an exact black hole solution. Following the same iterative procedure, we can approximate the metric to the second and next higher orders. However, we have to work out the properties of this metric (namely, the $r_{\rm EH}$, r_{ph}, and r_{ms}) order by order, which is not a desirable feature. In the next section, we consider another choice of equation of state, which will turn out to be more useful.

B. Case B: $2U+P=0$

In this section, we consider an interesting scenario where the dark radiation U and the dark pressure P satisfy the constraint $2U + P = 0$. For this specific choice, Eq. (21) leads to

$$\frac{dP}{dr} = -4\frac{P}{r}. \tag{48}$$

Therefore, the general solution for the dark pressure and the dark radiation is given by

$$P(r) = \frac{P_0}{r^4} \quad \text{and} \quad U(r) = -\frac{P_0}{2r^4}, \tag{49}$$

where P_0 is an arbitrary constant of integration. Consequently, from Eq. (22), the dark mass assumes the form

$$Q(r) = Q_0 + \frac{3\alpha P_0}{2r}, \tag{50}$$

with the integration constant Q_0. Using these forms for the source terms, the metric components can be computed, where

$$\begin{aligned} e^{\nu(r)} = e^{-\lambda(r)} &= 1 - \frac{2G_4M + Q_0}{r} - \frac{3\alpha P_0}{2r^2} + \frac{\mathcal{F}(R) - \Lambda_4}{3}r^2 \\ &= 1 - \frac{2G_4\tilde{M}}{r} + \frac{\tilde{\mathcal{Q}}}{r^2} - \frac{\tilde{\Lambda}}{3}r^2. \end{aligned} \tag{51}$$

This solution is interesting primarily because it represents an exact solution, which is very difficult to obtain in the presence of $f(R)$ gravity in higher dimensions. Although Eq. (51) resembles the de Sitter/anti–de Sitter Reissner-Nordström metric in general relativity, there are several differences. First, the ADM mass $\tilde{M}$ and the tidal charge parameter $\tilde{\mathcal{Q}}$ have completely different physical origins, i.e., have contributions from the nonlocal effects of the bulk Weyl tensor, which does not happen in general relativity. In Eq. (51), $\tilde{\mathcal{Q}}$ can assume both signatures, while in general relativity $\tilde{\mathcal{Q}}$ is always positive. The cosmological constant $\tilde{\Lambda}$ arises naturally in these models and owes its origin to $f(R)$ gravity in higher dimensions. Depending on the relative dominance of Λ_4 and $\mathcal{F}(R)$, $\tilde{\Lambda}$ can be positive, negative, or zero, such that the resultant metric is asymptotically de Sitter, anti–de Sitter, or flat. Recent cosmological observations of distant type Ia supernovae and the anisotropies in the cosmic microwave background radiation strongly indicate an accelerated expansion of the Universe [101–105], which can be explained by a repulsive cosmological constant with positive $\tilde{\Lambda}$. Therefore, it is essential to explore the ramifications of $\tilde{\Lambda}$ in various astrophysical situations. In what follows, we will investigate the influence of the cosmological constant in the continuum spectrum emitted by the accretion disk around quasars, which exhibit strong curvature effects near the horizon. Note, however, in our case, the origin of the cosmological constant is more physically motivated.

Again, for convenience of future computations, we redefine the metric components in terms of the gravitational radius, which for metric Eq. (51) is given by $r_g = G_4\tilde{M}$ (with $c = 1$), such that the metric components assume the form

$$e^{\nu(r)} = e^{-\lambda(r)} = 1 - \frac{2}{\tilde{r}} + \frac{q}{\tilde{r}^2} - \Lambda\tilde{r}^2, \tag{52}$$

where $q = \tilde{\mathcal{Q}}/r_g^2$ and $\Lambda = \tilde{\Lambda}r_g^2/3$.

IV. SPECTRUM FROM THE ACCRETION DISK AROUND BLACK HOLES IN THE BRANE EMBEDDED IN BULK $f(R)$ GRAVITY

In order to probe the observable effects of $f(R)$ gravity in higher dimensions, we consider the near horizon regime of quasars (which host supermassive black holes at the center), where deviations from general relativity is expected. The electromagnetic emission from the accretion disk around quasars bears the imprints of the background spacetime and hence can be used as a suitable tool to study the nature of strong gravity. In this section, we compute the signatures of higher dimensional $f(R)$ gravity in the continuum spectrum emitted by the accretion disk around quasars.

The continuum spectrum of black holes depends not only on the nature of the background spacetime but also on the characteristics of the accretion flow. Depending on the equation of state governing the dark radiation and the dark pressure, the background metric is given by Eqs. (42) and (47) or (51). For the present work, we will approximate the accretion flow in terms of the well-established "thin-disk model" [106,107], where the accreting fluid is assumed to be confined to the equatorial plane of the black hole, such that the resultant accretion disk is geometrically thin with $h(r) \ll r$ [$h(r)$ being the height of the disk at a radial distance r]. The azimuthal velocity u_ϕ of the accreting fluid dominates the radial velocity u_r and the vertical velocity u_z, such that $u_z \ll u_r \ll u_\phi$. Therefore, such systems do not harbor outflows. The presence of viscosity reduces the

angular momentum of the accreting fluid and generates a minimal amount of radial velocity, which facilitates slow inspiral and fall of matter into the black hole. The gravitational pull of the black hole is assumed to be much stronger compared to the radial pressure gradients and shear stresses, such that the accreting gas falls in nearly circular geodesics.

The energy-momentum tensor associated with the accreting fluid is given by

$$T^{\mu}_{\nu} = \rho_0(1+\Pi)u^{\mu}u_{\nu} + t^{\mu}_{\nu} + u^{\mu}q_{\nu} + q^{\mu}u_{\nu}, \tag{53}$$

where $\rho_0 u^{\mu}u^{\nu}$ is the stress tensor associated with the geodesic flow (ρ_0 being the proper density and u^{α} as the four velocity of the accreting fluid), $\Pi\rho_0 u^{\mu}u^{\nu}$ constitutes the stress-energy tensor from the specific internal energy (Π) of the system, $t^{\mu\nu}$ represents the energy-momentum tensor evaluated in the local inertial frame of the accreting fluid, and q^{μ} is the heat flux relative to the local rest frame. Note that both $t^{\mu\nu}$ and q^{μ} are orthogonal to the four velocity, such that $u^{\nu}t^{\mu}{}_{\nu} = 0 = u^{\mu}q_{\mu}$. In the thin-disk approximation, $\Pi \ll 1$, such that the special relativistic corrections to the local hydrodynamic, thermodynamic, and radiative properties of the fluid can be safely neglected. Therefore, the entire heat generated due to viscous dissipation is completely radiated away and the accreting fluid retains no heat. As a consequence, only the z component of the energy flux vector q^{α} has a nonzero contribution to the stress-energy tensor. For a more elaborate description of the thin accretion disk model, one is referred to [106–108].

The black hole is assumed to accrete at a steady rate $\dot{M}_0$ and the accreting fluid is assumed to obey conservation of mass, angular momentum, and energy. The conservation of mass is given by

$$\dot{M}_0 = -2\pi\sqrt{-g}\Sigma u^{r}, \tag{54}$$

where g represents the determinant of the metric whose effect on the spectrum we intend to study and Σ is the surface density of the accreting fluid. The conservation of angular momentum and energy assumes the forms

$$[\dot{M}_0 L - 2\pi\sqrt{-g}W^{r}_{\phi}]_{,r} = 4\pi\sqrt{-g}FL \tag{55}$$

and

$$[\dot{M}_0 E - 2\pi\sqrt{-g}\Omega W^{r}_{\phi}]_{,r} = 4\pi\sqrt{-g}FE, \tag{56}$$

respectively, where Ω is the angular velocity, $L = u_{\phi}$ is the specific angular momentum, and $E = -u_t$ is the specific energy of the accreting fluid. The flux from the disk is given by F, where

$$F \equiv \langle q^{z}(r,h)\rangle = \langle -q^{z}(r,-h)\rangle, \tag{57}$$

while the height-averaged stress tensor in the averaged rest frame is denoted by

$$\int_{-h}^{h} dz\langle t^{\alpha}_{\beta}\rangle = W^{\alpha}_{\beta}. \tag{58}$$

The conservation laws can be manipulated such that the flux $F(r)$ from the accretion disk is given by

$$F = \frac{\dot{M}_0}{4\pi\sqrt{-g}}\tilde{f}, \tag{59}$$

where

$$\tilde{f} = -\frac{\Omega_{,r}}{(E-\Omega L)^2}\left[EL - E_{ms}L_{ms} - 2\int_{r_{ms}}^{r} LE_{,r'}dr'\right]. \tag{60}$$

Equation (59) is derived by assuming that the viscous stress W^{r}_{ϕ} vanishes at the last stable circular orbit, such that the accretion disk truncates at r_{ms}. After crossing the marginally stable circular orbit, the accreting matter falls radially into the black hole.

By studying the geodesic motion of massive test particles in a given static, spherically symmetric spacetime, one can derive the angular velocity Ω, the specific energy E, and the specific angular momentum L in terms of the metric components, such that

$$\Omega = \frac{d\phi}{dt} = \frac{\sqrt{-\{g_{\phi\phi,r}\}\{g_{tt,r}\}}}{g_{\phi\phi,r}}, \tag{61}$$

$$E = -u_t = \frac{-g_{tt}}{\sqrt{-g_{tt} - \Omega^2 g_{\phi\phi}}}, \tag{62}$$

and

$$L = u_{\phi} = \frac{\Omega g_{\phi\phi}}{\sqrt{-g_{tt} - \Omega^2 g_{\phi\phi}}}. \tag{63}$$

In Eq. (60), r_{ms} represents the radius of the marginally stable circular orbit while E_{ms} and L_{ms} are specific energy and specific angular momentum at r_{ms}. The marginally stable circular orbit is obtained from the point of inflection of the effective potential V_{eff} in which the massive test particles move. Therefore, it is obtained from the relation $V_{\text{eff}} = V_{\text{eff},r} = V_{\text{eff},rr} = 0$, where V_{eff} is given by

$$V_{\text{eff}}(r) = \frac{E^2 g_{\phi\phi} + L^2 g_{tt}}{-g_{tt}g_{\phi\phi}} - 1. \tag{64}$$

Using Eqs. (62) and (63), Eq. (64) can be simplified to give Eq. (45), which can be solved to obtain r_{ms}.

The photons thus generated in the system undergo repeated collisions with the accreting gas, such that a thermal equilibrium is established between matter and radiation. Such an accretion disk is therefore geometrically thin but optically thick. Consequently, the disk radiates a Planck spectrum at every radial distance r with peak temperature given by $T(r) = (\tilde{F}(r)/\sigma)^{1/4}$, where $\tilde{F}(r) = F(r)c^6/G_4^2$

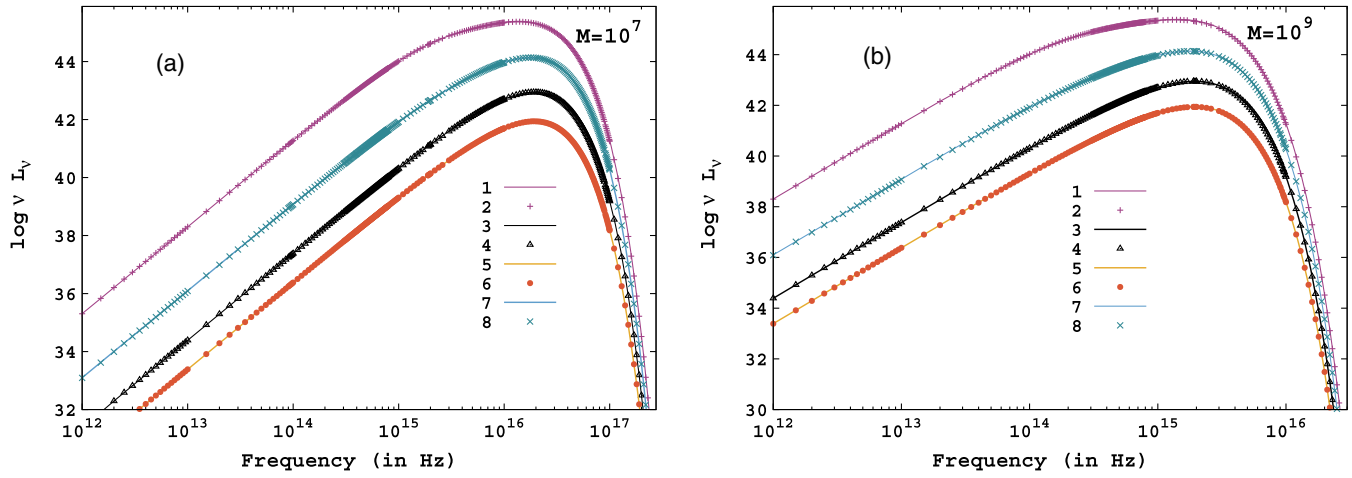

FIG. 1. The above figure illustrates variation of the theoretically derived luminosity from the accretion disk with frequency for two different masses of supermassive black holes. The background is given by Eqs. (46) and (47). Both (a) and (b) exhibit a set of eight spectra, which are drawn to explain the impact of various metric parameters on the theoretical spectrum. The metric parameters corresponding to spectra 1–8 are reported in Table I. The accretion rate assumed is 1 $M_\odot\,\mathrm{yr}^{-1}$ and $\cos i$ is taken to be 0.8.

(bringing back the G_4 and c) and σ denotes the Stefan-Boltzmann constant. By integrating the Planck function $B_\nu(T(r))$ over the disk surface, one can compute the luminosity L_ν from the disk at an observed frequency ν, such that

$$L_\nu = 8\pi^2 r_g^2 \cos i \int_{r_{\rm ms}}^{r_{\rm out}} \sqrt{-g_{rr}} B_\nu(T(\tilde{r}))\tilde{r}d\tilde{r} \quad \text{and}$$
$$B_\nu(T) = \frac{2h\nu^3/c^2}{\exp(\frac{h\nu}{z_g kT}) - 1}, \tag{65}$$

where r_g denotes the gravitational radius, i represents the inclination angle of the disk to the line of sight, and z_g is the gravitational redshift factor, which relates the modification induced in the photon frequency while traveling from the emitting material to the observer [109]. The gravitational redshift factor is given by

$$z_g = E\frac{\sqrt{-g_{tt} - \Omega^2 g_{\phi\phi}}}{E - \Omega L}. \tag{66}$$

Since the spectrum from the accretion disk is an envelope of a series of blackbody spectra emitted at different peak temperatures, it is often called a multicolor/multitemperature blackbody spectrum. Note that the theoretical spectrum depends chiefly on the g_{tt} component of the metric, while the g_{rr} component is required only during the integration of the flux to obtain the luminosity [see Eq. (65)] [108].

A. Effect of bulk $f(R)$ gravity on the emission from the accretion disk

In the present work, we are interested in investigating the modifications induced in the continuum spectrum of quasars due to the presence of $f(R)$ gravity in higher dimensions. The background spacetime is therefore given by Eqs. (46) and (47) for equation of state $P = 0$, while (52) denotes the background metric when the equation of state is given by $2U + P = 0$.

In Fig. 1, we plot the theoretically derived spectrum from the accretion disk when the equation of state is given by $P = 0$ for two different masses of supermassive black holes, namely, $10^7\ M_\odot$ [Fig. 1(a)] and $10^9\ M_\odot$ [Fig. 1(b)]. For each of the masses, eight spectra (1–8) are plotted in Fig. 1 by varying the various metric parameters in Eq. (47), which are detailed in Table I. In each of the spectra, the g_{tt} component is similar to the Schwarzschild spacetime [see Eq. (46)], while the g_{rr} component has several corrections to the Schwarzschild metric [see Eq. (47)]. From Table I, it is clear that the spectrum labeled by "1" corresponds to the Schwarzschild scenario, although the ADM mass owes its origin to $f(R)$ gravity in higher dimensions in the action. This difference in the origin of mass of the black hole cannot be perceived by an external observer. In spectrum 2, the spacetime is still Schwarzschild-like although the mass term in the g_{tt} and g_{rr} components of the metric are not the same.

TABLE I. Choice of metric parameters corresponding to spectra 1–8 in Fig. 1.

Spectrum	$\tilde{\varepsilon}$	$\tilde{\gamma}$	$\tilde{\eta}$	$\tilde{\sigma}$
1	2.0	0.0	0.0	0.0
2	0.5	0.0	0.0	0.0
3	2.0	9.0	0.0	1.0
4	2.0	10^{-7}	0.0	1.0
5	2.0	1.0	100.0	100.0
6	2.0	1.0	−100.0	100.0
7	2.0	1.0	1.0	10^{-6}
8	2.0	1.0	1.0	10^{-10}

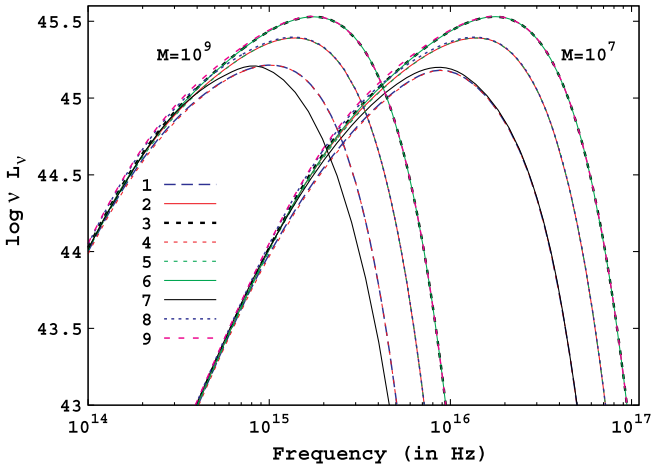

FIG. 2. The above figure illustrates effect of the metric Eq. (52) on the theoretically derived spectrum from the accretion disk for two different masses of supermassive black holes. The accretion rate assumed is 1 $M_\odot\,\mathrm{yr}^{-1}$ and $\cos i$ is taken to be 0.8.

From Fig. 1, it is clear that this change hardly affects the theoretical spectrum. In spectra 3 and 4, the mass term in g_{rr} is same as that of the g_{tt} component, while $\tilde{\sigma}$ and $\tilde{\gamma}$ are simultaneously changed as per Table I. Figure 1 shows that change of $\tilde{\sigma}$ has an important effect in the spectrum (since spectra 1 and 3 show deviations), while changing $\tilde{\gamma}$ barely has any impact (since spectra 3 and 4 are overlapping). For spectra 5–8, we fix $\tilde{\varepsilon}$ and $\tilde{\gamma}$, since we have understood their effect on the spectrum. Overlap of spectra 5 and 6 implies that $\tilde{\eta}$ has a negligible effect on the spectrum. The variation in spectra 1, 3, and 5 is chiefly due to the disparity in the values of $\tilde{\sigma}$. However, once $\tilde{\sigma}$ is lowered below 10^{-6} the spectrum becomes insensitive to the changes. This is inferred from the overlap of spectra 7 and 8.

Figure 2 depicts the variation of the theoretically derived luminosity with frequency for black hole masses $10^7\ M_\odot$ and $10^9\ M_\odot$ when the background spacetime is given by Eq. (52), which corresponds to the equation of state $2U + P = 0$. The values of the metric parameters corresponding to the nine spectra illustrated in Fig. 2 are given in Table II. Spectra 1, 4, and 7 correspond to a constant magnitude of $q = -3$, spectra 2, 5, and 8 are commensurate with $q = 0$, while spectra 3, 6, and 9 are in tandem with $q = 0.95$. For each set of constant q spectra, the cosmological constant Λ is variable according to Table II. From the virtual overlap of the spectra with constant q but variable Λ, it is quite explicit that the tidal charge parameter q has a more significant impact on the spectrum than the cosmological constant Λ. Only for $q = -3$ does the spectrum with $\Lambda < 0$ appear to be deviated from its $\Lambda \geq 0$ counterparts. Note that we cannot choose the magnitude of Λ arbitrarily large, as this is in odds with the cosmological observations [102,105]. On the other hand, if Λ is extremely small, it will hardly affect the spectrum. The magnitude of Λ should therefore be chosen in an optimal range.

TABLE II. Choice of metric parameters corresponding to spectra 1–9 in Fig. 2.

Spectrum	q	Λ
1	−3.0	0.0
2	0.0	0.0
3	0.95	0.0
4	−3.0	7×10^{-9}
5	0.0	7×10^{-9}
6	0.95	7×10^{-9}
7	−3.0	-2×10^{-7}
8	0.0	-2×10^{-7}
9	0.95	-2×10^{-7}

Moreover, from a theoretical point of view, there are restrictions on the maximum positive value of Λ. This stems from the fact that, unlike anti–de Sitter spacetime, a de Sitter spacetime has a cosmological horizon r_{CH} that is obtained from the largest solution of $e^{-\lambda(r)} = 0$ in Eq. (52). Our region of interest r should therefore be confined in the region $r_{\mathrm{EH}} < r < r_{CH}$, i.e., the outer radius of the accretion disk r_{out} should be within r_{CH}. The fact that the inner radius of the disk r_{in} truncates at r_{ms} automatically ensures that $r_{\mathrm{in}} > r_{\mathrm{EH}}$. With an enhancement in Λ, r_{CH} shrinks while r_{EH} increases, such that for $\Lambda = \Lambda_{\mathrm{max}} = 1/27$ (and $q = 0$) the two horizons coincide, and for higher values of Λ, the horizons disappear leading to the formation of a naked singularity [110]. The presence of q slightly modifies Λ_{max} with a negative q marginally lowering the value, as opposed to a positive q. Also note that we cannot arbitrarily increase q, once again to preserve the cosmic censorship conjecture. In the absence of Λ, the presence of an event horizon requires $q \leq 1$. On increasing the negative value of Λ, the maximum value of q gets marginally lowered (e.g., $q_{\mathrm{max}} \sim 0.925$ if $\Lambda \sim -0.1$), while the presence of a de Sitter Λ enhances the q_{max} (e.g., $q_{\mathrm{max}} \sim 1.01$ if $\Lambda \sim 0.05$). However, no real value of Λ can raise q_{max} up to 1.1. Therefore, for all practical purposes, we will confine ourselves to $\Lambda < 1/27$ and $q \leq 1$.

A more stringent constraint on Λ_{max} is established from the fact that no stable circular orbit exists for $\Lambda > 2.37 \times 10^{-4}$ in the absence of the charge parameter [110]. Once again, the presence of a negative q further lowers Λ_{max}, while a positive q raises this value up to a maximum of $\Lambda \sim 7 \times 10^{-4}$. Since our accretion disk truncates at r_{ms}, we need to keep the maximum value of Λ well below 2.37×10^{-4}. The choice of Λ automatically restricts the maximum extent of the accretion disk. This is because a positive Λ has a repulsive effect, as opposed to the attractive force offered by the central black hole. Therefore, the physically relevant region for accretion is the regime where the attractive force due to the black hole dominates. This is given by the static radius r_s, where the attractive force due to the black hole and the repulsive force due to Λ nullify. The value of r_s diminishes with an increase in Λ and is

evaluated from the turning point of the pseudo-Newtonian potential Ψ experienced by the test particles while moving in a given spacetime, in our case Eq. (52), where

$$\Psi = \int dr \frac{L^2}{E^2} r^3, \tag{67}$$

and E and L are given by Eqs. (62) and (63). The outer radius of the accretion disk $r_{\rm out}$ must be less than r_s for accretion to take place.

In this work, we will take $r_{\rm out} \sim 500 R_g$, which is just a typical choice [111,112]. This further brings down the maximum allowed value for $\Lambda \leq 7 \times 10^{-9} = \Lambda_{\rm max}$. Although the outer radius of the accretion disk can deviate from our choice, it will not affect the results substantially since a greater r_s (and hence a larger $r_{\rm out}$) will diminish $\Lambda_{\rm max}$ by orders of magnitude, which will have negligible effect on the spectrum. A smaller $r_{\rm out}$, on the other hand, will increase $\Lambda_{\rm max}$, but the effective disk luminosity will not change much since the flux is integrated over a smaller area of the disk. In fact, one can verify that by raising $\Lambda_{\rm max} \sim 10^{-6}$ the deviation from the Schwarzschild/Reissner-Nordström scenario [110,113] is minimal. Since the magnitude of Λ is very small, one needs to choose $r_{\rm out}$ judiciously in order to detect an observable effect of the cosmological constant on the spectrum.

A feature common to both Figs. 1 and 2 is that the disk luminosity of a lower mass black hole peaks at a higher frequency. This is because the peak temperature of the local blackbody emission is inversely proportional to the mass, $T(r) \propto M^{-1/4}$ [see discussion above Eq. (65)]. Hence, disk emission from stellar-mass black holes peak in soft x rays, while for supermassive black holes the maximum emission occurs in the optical domain. We also note that the spectra in Figs. 1 and 2 are different in the sense that the deviation from GR shows up in the low energy domain in Fig. 1 and high energy regime in Fig. 2. This is attributed to the fact that the g_{rr} term of the background metric governing Fig. 1 has a $\tilde{\sigma}\tilde{r}^4$ contribution in the denominator, which suppresses the luminosity from the Schwarzschild scenario. It is evident from Fig. 1 that even a minimal deviation of $\tilde{\sigma} \sim 10^{-6}$ causes a substantial departure from the general relativistic counterpart (see Table I and Fig. 1). The $\tilde{r}^4$ dependence of the g_{rr} component of the metric ensures that the outer disk, which emits in lower frequencies, has the dominant contribution in luminosity. Hence, the deviation from general relativity in Fig. 1 becomes evident in the lower frequencies. On the contrary, the metric components corresponding to Fig. 2 have inverse powers of $\tilde{r}$, hence deviations from GR are manifested chiefly in the inner disk, which emits high energy radiations.

V. NUMERICAL ANALYSIS

In this section, we use the thin-disk approximation for the accretion flow in the background spacetime given by Eq. (52), since this represents an exact black hole solution, to evaluate the theoretical estimates of optical luminosities for a sample of 80 Palomar-Green quasars [114,115]. We compute $L_{\rm opt} \equiv \nu L_\nu$ at the wavelength 4861 Å following Davis and Laor [115]. The masses of these quasars have been determined previously by the method of reverberation mapping [116–119], and for a small subsample of 13 quasars, the masses are also known by the $M - \sigma$ method [120–122]. The bolometric luminosities of these quasars have been estimated using observed data in the optical [123], UV [124], far-UV [125], and soft x-ray [126] domain. For all the quasars in the sample, the accretion rates and the observed estimates of the optical luminosity are reported in [115]. Since we are modeling the accretion disk of quasars whose emission peaks are in the optical part of the spectral energy distribution, we are primarily interested in accurate and precise estimates of the optical luminosity.

In order to compute the theoretical optical luminosity the inclination of the accretion disk, "i" is also required [Eq. (65)]. For quasars, "cos i" generally ranges from 0.5 to 1, since emissions from nearly edge-on systems are likely to be obscured. This permits us to neglect the effect of light bending while computing the spectrum from the accretion disk. Such effects become conspicuous for disks with high inclination angles [127,128]. In this work, we assume a typical value of $\cos i \sim 0.8$ for all the quasars [115]. This is further supported by the fact that the error (e.g., reduced χ^2, Nash-Sutcliffe efficiency, index of agreement, etc.) between the theoretical and observed luminosities for nonrotating black holes with a fixed q gets minimized when cosi lies between 0.77 and 0.82 [99]. The inclination angles of some of the quasars in our sample have been independently determined by Piotrovich *et al.* [129] by estimating the degree of polarization of the scattered radiation from the accretion disk. It turns out that their estimates are consistent with our choice.

In order to understand whether the presence of bulk $f(R)$ gravity provides a better approximation to the observed spectra, we calculate the theoretical estimates of the optical luminosity L_{opt} for all the 80 quasars with known masses, accretion rates, and disk inclination. This is compared with the corresponding observed values $L_{\rm obs}$ to deduce the most favored choice of the metric parameters (q and Λ) that explains observations the best. To arrive at the preferred model for q and Λ, we discuss several error estimators.

A. Chi square χ^2

If $\{\mathcal{O}_i\}$ represents a set of observed data with possible errors $\{\sigma_i\}$, and $\Omega_i(q, \Lambda)$ denotes the corresponding model estimates of the observed quantity with model parameters q and Λ, then the χ^2 of the distribution is given by

$$\chi^2(q, \Lambda) = \sum_i \frac{\{\mathcal{O}_i - \Omega_i(q, \Lambda)\}^2}{\sigma_i^2}. \tag{68}$$

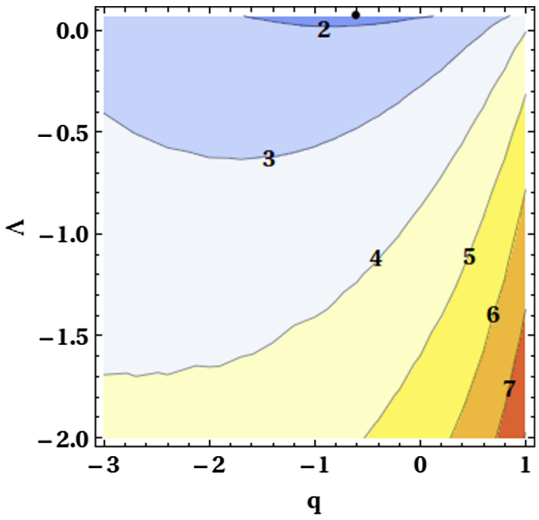

FIG. 3. Contours of constant χ^2 as a function of the metric parameters q and Λ. The values of Λ are in the units of $10^{-7}r_g^{-2}$. The minimum of the χ^2 is denoted by the black dot. It is evident from the plot that χ^2 minimizes for a negative value of $q \sim -0.6$ and a positive $\Lambda \sim \mathcal{O}(10^{-9})$. While a negative q marks a clear deviation from general relativity, a positive Λ indicates that a de Sitter spacetime is favored by electromagnetic observations from quasars.

For our sample, the error $\{\sigma_i\}$ corresponding to optical luminosities of individual quasars is not reported. Hence, we assign equal weight to every observation. The values of q and Λ that minimize χ^2 represent the most favored values of the metric parameters.

It is interesting to note that, although χ^2 turns out to be a valid error estimator, reduced chi square $\chi^2_{\text{Red}} = \chi^2/\nu$ (with ν being the degrees of freedom (d.o.f.)) is not useful in our case since the number of d.o.f. for our model is not very well defined. This is attributed to the fact that there are restrictions to the values of both q and Λ (see Sec. IV A). Such systems are known as models with prior where definition of d.o.f. requires additional input apart from the number of parameters in the model [130].

Figure 3 shows the constant χ^2 contours for different values of the metric parameters q and Λ. The values of the brane cosmological constant Λ are expressed in units of $10^{-7}r_g^{-2}$. From the figure, it is clear that χ^2 achieves a minimum value $\sim$1.78 (denoted by the black dot) for a negative tidal charge parameter $q \sim -0.6$ and a positive $\Lambda \sim 7 \times 10^{-9}$. Since general relativity cannot account for a negative tidal charge parameter, this may signal higher dimensions at play in the strong gravity regime around quasars. Note that the signature of q is more important than its exact value, since negative tidal charge parameters do not arise in general relativity. A positive Λ, on the other hand, signifies that a de Sitter spacetime is preferred from the continuum spectra of quasars. This is in agreement with the cosmological observations [102,105]. In the next section, we will comment on how the value of Λ estimated from our analysis compares with the cosmological constant measured from observations related to distant type Ia supernovae and cosmic microwave background radiation. Before that, we discuss a few more error estimators to confirm the robustness of our results.

B. Nash-Sutcliffe efficiency and its modified form

Nash-Sutcliffe efficiency E [131–133] is given by

$$E(q,\Lambda) = 1 - \frac{\sum_i \{\mathcal{O}_i - \Omega_i(q,\Lambda)\}^2}{\sum_i \{\mathcal{O}_i - \mathcal{O}_{av}\}^2}. \tag{69}$$

It relates the sum of the absolute squared differences between the theoretical predictions Ω_i and the observed values $\mathcal{O}_i$, normalized by the variance of the observed values. In Eq. (69), $\mathcal{O}_{av}$ denotes the mean observed optical luminosity of the quasars. E can assume a maximum value of 1. A model with $E \sim 1$ is ideal since it predicts the observations with greatest accuracy. From Eq. (69), it is clear that E can acquire negative values and may go up to $-\infty$. A model with negative E indicates that the average of the observed data is a better predictor than the model.

Since Nash-Sutcliffe efficiency E is susceptible to being oversensitive to higher values of the luminosity, a modified version of the same is proposed, which is denoted by E_1 [132]. This is due to the presence of the square of the error in the numerator in Eq. (69). Accordingly, the modified Nash-Sutcliffe efficiency E_1 is defined to be

$$E_1(q,\Lambda) = 1 - \frac{\sum_i |\mathcal{O}_i - \Omega_i(q,\Lambda)|}{\sum_i |\mathcal{O}_i - \mathcal{O}_{av}|}, \tag{70}$$

such that it succeeds to enhance the sensitivity of the estimator toward lower values of optical luminosity. Similar to E, the most favored model of q and Λ should maximize E_1.

In Figs. 4(a) and 4(b), we plot contours of constant E and E_1, respectively, as functions of q and Λ. As before, the black dot in both figures indicates the coordinates of maximum E and E_1. The figures explicitly elucidate that both the error estimators maximize for negative q and positive $\Lambda \sim \mathcal{O}(10^{-9})$, which is in agreement with our previous findings. This may be an indication of some new physics at play in the strong gravity regime: higher dimensions being one such possibility.

C. Index of agreement and its modified form

It turns out that the Nash-Sutcliffe efficiency and its modified form remain insensitive toward the differences between the observed and predicted means and variances. To overcome this shortcoming, the index of agreement is proposed [132–135]. It is denoted by d and assumes the following mathematical form:

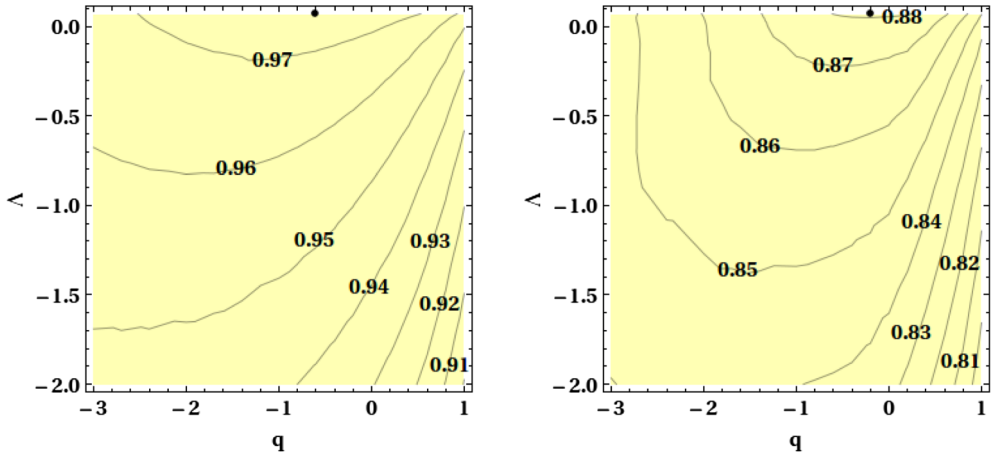

(a) Nash-Sutcliffe Efficiency (b) Modified Nash-Sutcliffe Efficiency

FIG. 4. Contours of constant (a) Nash-Sutcliffe efficiency E and (b) the modified form of the Nash-Sutcliffe efficiency E_1 with the tidal charge parameter q and Λ. As before, the values of Λ are in units of $10^{-7}r_g^{-2}$. Both the error estimators maximize for negative values of q and positive $\Lambda \sim \mathcal{O}(10^{-9})$.

$$d(q,\Lambda) = 1 - \frac{\sum_i \{\mathcal{O}_i - \Omega_i(q,\Lambda)\}^2}{\sum_i \{|\mathcal{O}_i - \mathcal{O}_{av}| + |\Omega_i(q,\Lambda) - \mathcal{O}_{av}|\}^2}. \quad (71)$$

The denominator, often known as the potential error, denotes the maximum deviation of each pair of observed and predicted luminosities from the average luminosity.

Again, due to the presence of square terms in the numerator, the index of agreement suffers from oversensitivity to higher values of optical luminosity, and hence, its modified version d_1 is proposed, where

$$d_1(q,\Lambda) = 1 - \frac{\sum_i |\mathcal{O}_i - \Omega_i(q,\Lambda)|}{\sum_i \{|\mathcal{O}_i - \mathcal{O}_{av}| + |\Omega_i(q,\Lambda) - \mathcal{O}_{av}|\}}. \quad (72)$$

From Eqs. (71) and (72), it is clear that the best model for q and Λ corresponds to the maximum value for d and d_1, which cannot be greater than 1. Since the denominators in Eqs. (71) and (72) are greater than Eqs. (69) and (70), respectively, the index of agreement and its modified form always assume greater values compared to E and E_1. Figures 5(a) and 5(b) illustrate the constant contours of d and d_1 with variation in q and Λ. From the coordinates of the black dot, which denote the maximum of E and E_1, it is clear that the index of agreement and its modified form also attain a maxima for a negative value of q and a positive Λ. The maximum value of d and d_1 is achieved for $q \sim -0.6$ and $q \sim -0.2$, respectively. The value of Λ that maximizes d and d_1 corresponds to $7 \times 10^{-9}r_g^{-2}$. Since Figs. 5(a) and 5(b) replicate the trend exhibited by Figs. 4(a) and 4(b), respectively, the conclusions drawn previously remain unaltered. Therefore, the behavior of the error

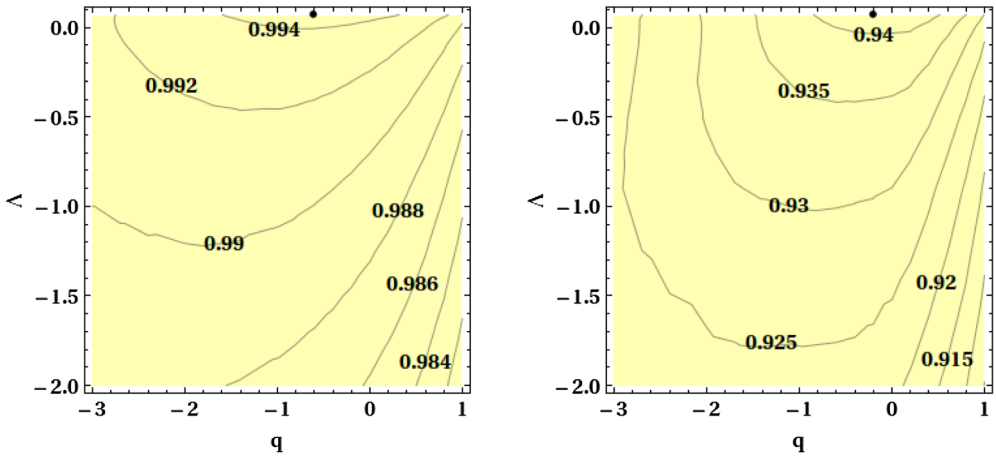

(a) Index of agreement (b) Modified index of agreement

FIG. 5. Contours of constant (a) index of agreement d and (b) its modified form d_1 with variations in the tidal charge parameter q and brane cosmological constant Λ. The black dot indicates the values of q and Λ, where d and d_1 attain the maximum. Both the error estimators maximize for negative values of q and positive $\Lambda \sim \mathcal{O}(10^{-9})$. Note that the values of Λ are in units of $10^{-7}r_g^{-2}$.

estimators indicate that a negative tidal charge parameter and a positive Λ is favored by optical observations of quasars.

VI. SUMMARY AND CONCLUSIONS

In this work, our chief goal was to extricate the imprints of bulk $f(R)$ gravity from the quasar continuum spectrum, which are ideal astrophysical probes to explore the nature of gravitational interaction in extreme situations. Extra dimensions and higher curvature corrections are often believed to be manifestations of the ultraviolet nature of gravity, with interesting consequences in inflationary cosmology, late-time cosmic acceleration, gravitational waves, and collider physics. Hence, it is instructive to investigate their impact on the electromagnetic spectrum emitted by the accretion disk around quasars, which are expected to exhibit maximum curvature effects, especially near the horizon. The presence of $f(R)$ gravity in higher dimensions substantially modifies the effective gravitational field equations on the brane, such that they evince significant deviations from Einstein's equations. Even in the absence of any matter energy on the brane, the electric part of the Weyl tensor, which represents the nonlocal gravitational effects of the bulk, acts a source for gravity in four dimensions. In addition, the interplay of the bulk cosmological constant, brane tension, and higher curvature terms in the bulk action naturally induce a cosmological constant in the brane, whose origin is physically motivated. A positive cosmological constant is often invoked to interpret the observations related to distant type Ia supernovae and the anisotropies in the cosmic microwave background radiation, which signifies an accelerated expansion of the Universe. Therefore, the effect of such a term in the black hole continuum spectrum is worth exploring.

As a first approximation, static, spherically symmetric and vacuum solutions of these modified field equations are explored since they represent the simplest deviation from the standard Schwarzschild scenario in general relativity. These approximations permit a decomposition of the electric part of the Weyl tensor into dark radiation and dark pressure, such that various equations of state connecting them lead to different classes of black hole solutions. We consider two such solutions in this work, corresponding to equations of state $P = 0$ and $2U + P = 0$. While the former leads to a perturbative solution, the latter assumes an exact black hole spacetime, bearing a striking resemblance to the Reissner-Nordström–de Sitter/anti–de Sitter/flat metric in general relativity. The asymptotic character of the exact solution is determined by the signature and the magnitude of the brane cosmological constant, while the trademark of extra dimensions is encoded in the charge parameter, which can assume a negative sign, unlike GR. Although we analyze the effect of both backgrounds on the quasar continuum spectrum, we perform a comparison with observations only with the exact spacetime, since the perturbative background is subject to vary with higher order corrections to the metric.

It is important to note that the exact solution is characterized by two parameters, namely, the tidal charge parameter and the brane cosmological constant. In a previous work [99], we explored the sole impact of the charge parameter on the continuum spectrum of 80 quasars to infer that optical observations of quasars favor a negative charge parameter. This work is subsequently generalized to axisymmetric spacetimes [136], where the metric resembles the familiar Kerr-Newmann solution in GR. Inclusion of black hole rotation not only corroborates our earlier finding, but also enables us to estimate the spin of the quasars [136]. This is further supported by the study of quasiperiodic oscillations in the black hole power spectrum, where a negative charge parameter is reported to be favored by observations [137].

The present work aims to examine the effect of the charge parameter on the continuum spectrum in the presence of the brane cosmological constant. In order to accomplish this, we compute the theoretical estimates of optical luminosity for the sample of 80 quasars by varying the two relevant metric parameters (q and Λ) and compare them with the corresponding observed values. By computing several error estimators, namely, chi squared, Nash-Sutcliffe efficiency, index of agreement, and the modified versions of the last two, we conclude that optical observations of quasars indeed favor a negative tidal charge parameter and a small positive Λ. A negative charge parameter that potentially arises in a higher dimensional scenario marks a clear deviation from general relativity and this is in accordance with our previous findings. A positive Λ, on the other hand, is in concordance with the aforementioned cosmological observations. We further mention that the tidal charge is related to the compactification scale of the extra dimension since the signature and magnitude of q determines the extent of the extra dimension as well as the penetration of the horizon of the black hole into the bulk spacetime [138]. This is achieved by evolving the brane metric to the bulk, which involves studying the evolution of the extrinsic curvature along the extra dimension. In particular, negative values of q modify the bulk metric from a black string to a black cigar, thereby making the extra dimension more compactified and hence seeming to be more natural [138]. In particular, the observationally favored value of $q \sim -0.6$ makes the extra dimension compactified by 1% compared to the general relativistic scenario. The compactification scale, however, continues to be the Planck scale.

Our analysis also enables us to provide an estimate of the magnitude of Λ from the quasar optical data, which turns out to be $\mathcal{O}(10^{-9})$ in units of inverse squared of the gravitational radius r_g. Since r_g varies with the mass of the quasar, it might appear that Λ deduced by us is mass dependent. However, one can verify that this choice of units

does not affect the order of magnitude estimate of Λ, which is based on the maximum mass $M_{\max}$ of the quasar in the sample. For lower mass quasars with mass M, we should have ideally chosen a cosmological constant $M^2/M_{\max}^2$ times smaller than the Λ of $M_{\max}$ while performing the error analysis. Since Λ is inherently very tiny, one can check that it will be even smaller for the low mass quasars, and therefore, their impact on the spectrum will be negligible. With $M_{\max} \sim 10^9\ M_\odot$, it can be shown that $\Lambda \sim 10^{-38}\ \mathrm{cm}^{-2}$ and it is remarkable that such a tiny value of the cosmological constant can be discerned from the accretion data. A variation of the outer radius r_{out} allows us to consider a marginally higher value for the repulsive Λ, which enhances the magnitude of estimated Λ roughly by an order. Our analysis, therefore, establishes a strong constraint on the upper limit of Λ from the quasar optical data. Note that this is a much stronger constraint compared to the work of Pérez *et al.* [113], which is based on the observation of only a single stellar-mass black hole source Cygnus X-1. With enhanced precision in observing the inner regions of the disk by future telescopes and including the effects of the corona in modeling the spectral energy distribution of the quasars, a tighter constraint on Λ can be established. A similar analysis on a different sample of quasars and microquasars with known masses and accretion rates is also worth exploring.

ACKNOWLEDGMENTS

The research of S. S. G. is partially supported by the Science and Engineering Research Board-Extra Mural Research (Grant No. EMR/2017/001372), Government of India. The authors thank Dr. Sumanta Chakraborty for useful comments and discussions throughout the course of this work.

[1] C. M. Will, Was Einstein right?, Ann. Phys. (Amsterdam) **15**, 19 (2005); **518**, 19 (2006).
[2] C. M. Will, The confrontation between general relativity and experiment, Living Rev. Relativity **9**, 3 (2006).
[3] N. Yunes and X. Siemens, Gravitational-wave tests of general relativity with ground-based detectors and Pulsar timing-arrays, Living Rev. Relativity **16**, 9 (2013).
[4] K. Akiyama *et al.* (Event Horizon Telescope Collaboration), First M87 Event Horizon Telescope Results. I. The shadow of the supermassive black hole, Astrophys. J. **875**, L1 (2019).
[5] K. Akiyama *et al.* (Event Horizon Telescope Collaboration), First M87 Event Horizon Telescope Results. VI. The shadow and mass of the central black hole, Astrophys. J. **875**, L6 (2019).
[6] D. Ayzenberg and N. Yunes, Black hole shadow as a test of general relativity: Quadratic gravity, Classical Quantum Gravity **35**, 235002 (2018).
[7] R. Penrose, Gravitational Collapse and Space-Time Singularities, Phys. Rev. Lett. **14**, 57 (1965).
[8] S. W. Hawking, Breakdown of predictability in gravitational collapse, Phys. Rev. D **14**, 2460 (1976).
[9] D. Christodoulou, The formation of black holes and singularities in spherically symmetric gravitational collapse, Commun. Pure Appl. Math. **44**, 339 (1991).
[10] M. Milgrom, A modification of the Newtonian dynamics: Implications for galaxies, Astrophys. J. **270**, 371 (1983).
[11] J. Bekenstein and M. Milgrom, Does the missing mass problem signal the breakdown of Newtonian gravity?, Astrophys. J. **286**, 7 (1984).
[12] M. Milgrom and R. H. Sanders, MOND and the dearth of dark matter in ordinary elliptical galaxies', Astrophys. J. **599**, L25 (2003).
[13] S. Perlmutter *et al.* (Supernova Cosmology Project Collaboration), Measurements of Omega and Lambda from 42 high redshift supernovae, Astrophys. J. **517**, 565 (1999).
[14] A. G. Riess *et al.* (Supernova Search Team Collaboration), Observational evidence from supernovae for an accelerating universe and a cosmological constant, Astron. J. **116**, 1009 (1998).
[15] C. Rovelli, Black Hole Entropy from Loop Quantum Gravity, Phys. Rev. Lett. **77**, 3288 (1996).
[16] F. Dowker, Causal sets and the deep structure of spacetime, in 100 Years of Relativity: Space-Time Structure: Einstein and Beyond, edited by A. Ashtekar (World Scientific, 2005), pp. 445–464.
[17] A. Ashtekar, T. Pawlowski, and P. Singh, Quantum Nature of the Big Bang, Phys. Rev. Lett. **96**, 141301 (2006).
[18] S. Nojiri and S. D. Odintsov, Unified cosmic history in modified gravity: from F(R) theory to Lorentz non-invariant models, Phys. Rep. **505**, 59 (2011).
[19] S. Nojiri and S. D. Odintsov, Modified f(R) gravity consistent with realistic cosmology: From matter dominated epoch to dark energy universe, Phys. Rev. D **74**, 086005 (2006).
[20] S. Capozziello, S. Nojiri, S. D. Odintsov, and A. Troisi, Cosmological viability of f(R)-gravity as an ideal fluid and its compatibility with a matter dominated phase, Phys. Lett. **639B**, 135 (2006).
[21] S. Bahamonde, S. D. Odintsov, V. K. Oikonomou, and M. Wright, Correspondence of $F(R)$ gravity singularities in Jordan and Einstein frames, Ann. Phys. (Amsterdam) **373**, 96 (2016).
[22] C. Lanczos, Electricity as a natural property of Riemannian geometry, Rev. Mod. Phys. **39**, 716 (1932).

[23] C. Lanczos, A remarkable property of the Riemann-Christoffel tensor in four dimensions, Ann. Math. **39**, 842 (1938).
[24] D. Lovelock, The Einstein tensor and its generalizations, J. Math. Phys. (N.Y.) **12**, 498 (1971).
[25] T. Padmanabhan and D. Kothawala, Lanczos-Lovelock models of gravity, Phys. Rep. **531**, 115 (2013).
[26] N. Dadhich, R. Durka, N. Merino, and O. Miskovic, Dynamical structure of pure Lovelock gravity, Phys. Rev. D **93**, 064009 (2016).
[27] T. Shiromizu, K.-i. Maeda, and M. Sasaki, The Einstein equation on the 3-brane world, Phys. Rev. D **62**, 024012 (2000).
[28] N. Dadhich, R. Maartens, P. Papadopoulos, and V. Rezania, Black holes on the brane, Phys. Lett. B **487**, 1 (2000).
[29] T. Harko and M. K. Mak, Vacuum solutions of the gravitational field equations in the brane world model, Phys. Rev. D **69**, 064020 (2004).
[30] T. R. P. Carames, M. E. X. Guimaraes, and J. M. Hoff da Silva, Effective gravitational equations for $f(R)$ brane-world models, Phys. Rev. D **87**, 106011 (2013).
[31] Z. Haghani, H. R. Sepangi, and S. Shahidi, Cosmological dynamics of brane f(R) gravity, J. Cosmol. Astropart. Phys. 02 (2012) 031.
[32] S. Chakraborty and S. SenGupta, Spherically symmetric brane spacetime with bulk $f(\mathcal{R})$ gravity, Eur. Phys. J. C **75**, 11 (2015).
[33] S. Chakraborty and S. SenGupta, Effective gravitational field equations on m-brane embedded in n-dimensional bulk of Einstein and $f(\mathcal{R})$ gravity, Eur. Phys. J. C **75**, 538 (2015).
[34] C. Brans and R. H. Dicke, Mach's principle and a relativistic theory of gravitation, Phys. Rev. **124**, 925 (1961).
[35] G. W. Horndeski, Second-order scalar-tensor field equations in a four-dimensional space, Int. J. Theor. Phys. **10**, 363 (1974).
[36] T. P. Sotiriou and S.-Y. Zhou, Black Hole Hair in Generalized Scalar-Tensor Gravity, Phys. Rev. Lett. **112**, 251102 (2014).
[37] E. Babichev, C. Charmousis, and A. Lehbel, Black holes and stars in Horndeski theory, Classical Quantum Gravity **33**, 154002 (2016).
[38] T. P. Sotiriou and V. Faraoni, f(R) Theories of gravity, Rev. Mod. Phys. **82**, 451 (2010).
[39] A. De Felice and S. Tsujikawa, f(R) theories, Living Rev. Relativity **13**, 3 (2010).
[40] S. Chakraborty and S. SenGupta, Spherically symmetric brane spacetime with bulk f(r) gravity, Eur. Phys. J. C **75**, 11 (2015).
[41] K. Bamba and S. D. Odintsov, Inflation and late-time cosmic acceleration in non-minimal Maxwell-$F(R)$ gravity and the generation of large-scale magnetic fields, J. Cosmol. Astropart. Phys. 04 (2008) 024.
[42] A. de la Cruz-Dombriz and A. Dobado, A f(R) gravity without cosmological constant, Phys. Rev. D **74**, 087501 (2006).
[43] A. A. Starobinsky, A new type of isotropic cosmological models without singularity, Phys. Lett. **91B**, 99 (1980).
[44] S. Nojiri and S. D. Odintsov, The future evolution and finite-time singularities in F(R)-gravity unifying the inflation and cosmic acceleration, Phys. Rev. D **78**, 046006 (2008).
[45] S. Capozziello, V. F. Cardone, and A. Troisi, Dark energy and dark matter as curvature effects, J. Cosmol. Astropart. Phys. 08 (2006) 001.
[46] S. Capozziello, V. F. Cardone, and A. Troisi, Low surface brightness galaxies rotation curves in the low energy limit of r**n gravity: No need for dark matter?, Mon. Not. R. Astron. Soc. **375**, 1423 (2007).
[47] C. Corda, Interferometric detection of gravitational waves: The definitive test for general relativity, Int. J. Mod. Phys. D **18**, 2275 (2009).
[48] C. Corda, S. A. Ali, and C. Cafaro, Interferometer response to scalar gravitational waves, Int. J. Mod. Phys. D **19**, 2095 (2010).
[49] C. Corda, Primordial production of massive relic gravitational waves from a weak modification of general relativity, Astropart. Phys. **30**, 209 (2008).
[50] S. Nojiri and S. D. Odintsov, Newton law corrections and instabilities in f(R) gravity with the effective cosmological constant epoch, Phys. Lett. B **652**, 343 (2007).
[51] S. Nojiri and S. D. Odintsov, Unifying inflation with LambdaCDM epoch in modified f(R) gravity consistent with Solar System tests, Phys. Lett. B **657**, 238 (2007).
[52] S. Nojiri and S. D. Odintsov, Modified f(R) gravity unifying R**m inflation with Lambda CDM epoch, Phys. Rev. D **77**, 026007 (2008).
[53] S. Capozziello and A. Troisi, PPN-limit of fourth order gravity inspired by scalar-tensor gravity, Phys. Rev. D **72**, 044022 (2005).
[54] S. Capozziello, A. Stabile, and A. Troisi, The Newtonian limit of f(R) gravity, Phys. Rev. D **76**, 104019 (2007).
[55] S. Capozziello, A. Stabile, and A. Troisi, Fourth-order gravity and experimental constraints on Eddington parameters, Mod. Phys. Lett. A **21**, 2291 (2006).
[56] G. Nordstrom, On the possibility of unifying the electromagnetic and the gravitational fields, Phys. Z. **15**, 504 (1914).
[57] T. Kaluza, Zum unittsproblem der physik, Sitzungsber. Preuss. Akad. Wiss. Berlin, Math. Phys. **1921**, 966 (1921) [Int. J. Mod. Phys. D **27**, 1870001 (2018)].
[58] O. Klein, The Aatomicity of electricity as a quantum theory law, Nature (London) **118**, 516 (1926).
[59] P. Horava and E. Witten, Heterotic and type I string dynamics from eleven-dimensions, Nucl. Phys. **B460**, 506 (1996).
[60] J. Polchinski, *String Theory. Vol. 1: An Introduction to the Bosonic String*, Cambridge Monographs on Mathematical Physics (Cambridge University Press, Cambridge, England, 2007).
[61] J. Polchinski, *String Theory. Vol. 2: Superstring Theory and Beyond*, Cambridge Monographs on Mathematical Physics (Cambridge University Press, Cambridge, England, 2007).
[62] I. Antoniadis, A possible new dimension at a few TeV, Phys. Lett. B **246**, 377 (1990).
[63] N. Arkani-Hamed, S. Dimopoulos, and G. R. Dvali, The hierarchy problem and new dimensions at a millimeter, Phys. Lett. B **429**, 263 (1998).

[64] I. Antoniadis, N. Arkani-Hamed, S. Dimopoulos, and G. R. Dvali, New dimensions at a millimeter to a Fermi and superstrings at a TeV, Phys. Lett. B **436**, 257 (1998).

[65] L. Randall and R. Sundrum, A Large Mass Hierarchy from a Small Extra Dimension, Phys. Rev. Lett. **83**, 3370 (1999).

[66] C. Csaki, M. Graesser, L. Randall, and J. Terning, Cosmology of brane models with radion stabilization, Phys. Rev. D **62**, 045015 (2000).

[67] L. Randall and R. Sundrum, An Alternative to Compactification, Phys. Rev. Lett. **83**, 4690 (1999).

[68] J. Garriga and T. Tanaka, Gravity in the Brane World, Phys. Rev. Lett. **84**, 2778 (2000).

[69] N. Arkani-Hamed, S. Dimopoulos, and G. R. Dvali, Phenomenology, astrophysics and cosmology of theories with submillimeter dimensions and TeV scale quantum gravity, Phys. Rev. D **59**, 086004 (1999).

[70] H. Davoudiasl, J. L. Hewett, and T. G. Rizzo, Bulk gauge fields in the Randall-Sundrum model, Phys. Lett. B **473**, 43 (2000).

[71] H. Davoudiasl, J. L. Hewett, and T. G. Rizzo, Experimental probes of localized gravity: On and off the wall, Phys. Rev. D **63**, 075004 (2001).

[72] H. Davoudiasl, J. L. Hewett, and T. G. Rizzo, Phenomenology of the Randall-Sundrum Gauge Hierarchy Model, Phys. Rev. Lett. **84**, 2080 (2000).

[73] R. S. Hundi and S. SenGupta, Fermion mass hierarchy in a multiple warped braneworld model, J. Phys. G **40**, 075002 (2013).

[74] S. Chakraborty and S. SenGupta, Higher curvature gravity at the LHC, Phys. Rev. D **90**, 047901 (2014).

[75] S. Dimopoulos and G. L. Landsberg, Black Holes at the LHC, Phys. Rev. Lett. **87**, 161602 (2001).

[76] T. Banks and W. Fischler, A model for high-energy scattering in quantum gravity, arXiv:hep-th/9906038.

[77] S. Pal, S. Bharadwaj, and S. Kar, Can extra dimensional effects replace dark matter?, Phys. Lett. B **609**, 194 (2005).

[78] C. G. Boehmer and T. Harko, On Einstein clusters as galactic dark matter halos, Mon. Not. R. Astron. Soc. **379**, 393 (2007).

[79] T. Harko and K. S. Cheng, The Virial theorem and the dynamics of clusters of galaxies in the brane world models, Phys. Rev. D **76**, 044013 (2007).

[80] S. Chakraborty and S. SenGupta, Kinematics of Radion field: A possible source of dark matter, Eur. Phys. J. C **76**, 648 (2016).

[81] A. Lukas, B. A. Ovrut, and D. Waldram, Boundary inflation, Phys. Rev. D **61**, 023506 (1999).

[82] N. Arkani-Hamed, S. Dimopoulos, N. Kaloper, and J. March-Russell, Rapid asymmetric inflation and early cosmology in theories with submillimeter dimensions, Nucl. Phys. **B567**, 189 (2000).

[83] K. R. Dienes, E. Dudas, T. Gherghetta, and A. Riotto, Cosmological phase transitions and radius stabilization in higher dimensions, Nucl. Phys. **B543**, 387 (1999).

[84] A. Mazumdar and J. Wang, A note on brane inflation, Phys. Lett. B **490**, 251 (2000).

[85] S. Chakraborty and S. Sengupta, Radion cosmology and stabilization, Eur. Phys. J. C **74**, 3045 (2014).

[86] N. Banerjee and T. Paul, Inflationary scenario from higher curvature warped spacetime, Eur. Phys. J. C **77**, 672 (2017).

[87] I. Banerjee, S. Chakraborty, and S. SenGupta, Radion induced inflation on nonflat brane and modulus stabilization, Phys. Rev. D **99**, 023515 (2019).

[88] K. Koyama, Cosmic Microwave Radiation Anisotropies in Brane Worlds, Phys. Rev. Lett. **91**, 221301 (2003).

[89] A. Mazumdar, Interesting consequences of brane cosmology, Phys. Rev. D **64**, 027304 (2001).

[90] R. Maartens, Cosmological dynamics on the brane, Phys. Rev. D **62**, 084023 (2000).

[91] R. Maartens, Brane world gravity, Living Rev. Relativity **7**, 7 (2004).

[92] P. Binetruy, C. Deffayet, and D. Langlois, Nonconventional cosmology from a brane universe, Nucl. Phys. **B565**, 269 (2000).

[93] C. Csaki, M. Graesser, C. F. Kolda, and J. Terning, Cosmology of one extra dimension with localized gravity, Phys. Lett. B **462**, 34 (1999).

[94] D. Bazeia, R. Menezes, A. Yu. Petrov, and A. J. da Silva, On the many-field $f(R)$ brane, Phys. Lett. B **726**, 523 (2013).

[95] A. Borzou, H. R. Sepangi, S. Shahidi, and R. Yousefi, Brane f(R) gravity, Europhys. Lett. **88**, 29001 (2009).

[96] T. Padmanabhan, *Gravitation: Foundations and Frontiers* (Cambridge University Press, Cambridge, England, 2010).

[97] C. Germani and R. Maartens, Stars in the brane world, Phys. Rev. D **64**, 124010 (2001).

[98] A. N. Aliev and A. E. Gumrukcuoglu, Charged rotating black holes on a 3-brane, Phys. Rev. D **71**, 104027 (2005).

[99] I. Banerjee, S. Chakraborty, and S. SenGupta, Excavating black hole continuum spectrum: Possible signatures of scalar hairs and of higher dimensions, Phys. Rev. D **96**, 084035 (2017).

[100] R. Maartens, Geometry and dynamics of the brane world, in *Spanish Relativity Meeting on Reference Frames and Gravitomagnetism (EREs2000) Valladolid, Spain, 2000* (World Scientific, 2001).

[101] N. A. Bahcall, J. P. Ostriker, S. Perlmutter, and P. J. Steinhardt, The cosmic triangle: Assessing the state of the universe, Science **284**, 1481 (1999).

[102] D. N. Spergel *et al.* (WMAP Collaboration), First year Wilkinson microwave anisotropy probe (WMAP) observations: Determination of cosmological parameters, Astrophys. J. Suppl. Ser. **148**, 175 (2003).

[103] D. N. Spergel *et al.* (WMAP Collaboration), Wilkinson microwave anisotropy probe (WMAP) three year results: Implications for cosmology, Astrophys. J. Suppl. Ser. **170**, 377 (2007).

[104] P. A. R. Ade *et al.* (Planck Collaboration), Planck 2015 results. XIV. Dark energy and modified gravity, Astron. Astrophys. **594**, A14 (2016).

[105] P. A. R. Ade *et al.* (Planck Collaboration), Planck 2015 results. XIII. Cosmological parameters, Astron. Astrophys. **594**, A13 (2016).

[106] I. D. Novikov and K. S. Thorne, Astrophysics of black holes, in *Black Holes (Les Astres Occlus)*, edited by C. Dewitt and B. S. Dewitt (Gordon and Breach, New York, 1973), pp. 343–450.

[107] D. N. Page and K. S. Thorne, Disk-accretion onto a black hole. Time-averaged structure of accretion disk, Astrophys. J. **191**, 499 (1974).
[108] I. Banerjee, B. Mandal, and S. SenGupta, In quest of axionic hairs in quasars, J. Cosmol. Astropart. Phys. 03 (2018) 039.
[109] D. Ayzenberg and N. Yunes, Black hole continuum spectra as a test of general relativity: Quadratic gravity, Classical Quantum Gravity **34**, 115003 (2017).
[110] Z. Stuchlik and J. Kovar, Pseudo-Newtonian gravitational potential for Schwarzschild-de Sitter spacetimes, Int. J. Mod. Phys. D **17**, 2089 (2008).
[111] D. J. Walton, E. Nardini, A. C. Fabian, L. C. Gallo, and R. C. Reis, Suzaku observations of 'bare' active galactic nuclei, Mon. Not. R. Astron. Soc. **428**, 2901 (2013).
[112] C. Bambi and E. Barausse, Constraining the quadrupole moment of stellar-mass black-hole candidates with the continuum fitting method, Astrophys. J. **731**, 121 (2011).
[113] D. Pérez, G. E. Romero, and S. E. P. Bergliaffa, Accretion disks around black holes in modified strong gravity, Astron. Astrophys. **551**, A4 (2013).
[114] M. Schmidt and R. F. Green, Quasar evolution derived from the Palomar bright quasar survey and other complete quasar surveys, Astrophys. J. **269**, 352 (1983).
[115] S. W. Davis and A. Laor, The radiative efficiency of accretion flows in individual AGN, Astrophys. J. **728**, 98 (2011).
[116] S. Kaspi, P. S. Smith, H. Netzer, D. Maoz, B. T. Jannuzi, and U. Giveon, Reverberation measurements for 17 quasars and the size mass luminosity relations in active galactic nuclei, Astrophys. J. **533**, 631 (2000).
[117] S. Kaspi, D. Maoz, H. Netzer, B. M. Peterson, M. Vestergaard, and B. T. Jannuzi, The relationship between luminosity and broad-line region size in active galactic nuclei, Astrophys. J. **629**, 61 (2005).
[118] T. A. Boroson and R. F. Green, The emission—line properties of low—redshift quasi-stellar objects, Astrophys. J. Suppl. Ser. **80**, 109 (1992).
[119] B. M. Peterson *et al.*, Central masses and broad-line region sizes of active galactic nuclei. II. A Homogeneous analysis of a large reverberation-mapping database, Astrophys. J. **613**, 682 (2004).
[120] L. Ferrarese and D. Merritt, A Fundamental relation between supermassive black holes and their host galaxies, Astrophys. J. **539**, L9 (2000).
[121] K. Gebhardt *et al.*, A relationship between nuclear black hole mass and galaxy velocity dispersion, Astrophys. J. **539**, L13 (2000).
[122] S. Tremaine *et al.*, The slope of the black hole mass versus velocity dispersion correlation, Astrophys. J. **574**, 740 (2002).
[123] G. Neugebauer, R. F. Green, K. Matthews, M. Schmidt, B. T. Soifer, and J. Bennett, Continuum energy distributions of quasars in the Palomar-Green Survey, Astrophys. J. **63**, 615 (1987).
[124] A. Baskin and A. Laor, What controls the C IV line profile in active galactic nuclei?, Mon. Not. R. Astron. Soc. **356**, 1029 (2005).
[125] J. E. Scott, G. A. Kriss, M. Brotherton, R. F. Green, J. Hutchings, J. M. Shull, and W. Zheng, A Composite extreme ultraviolet QSO spectrum from FUSE, Astrophys. J. **615**, 135 (2004).
[126] W. N. Brandt, A. Laor, and B. J. Wills, On the nature of soft x-ray weak quasistellar objects, Astrophys. J. **528**, 637 (2000).
[127] C. Bambi, A code to compute the emission of thin accretion disks in non-Kerr space-times and test the nature of black hole candidates, Astrophys. J. **761**, 174 (2012).
[128] L. Kong, Z. Li, and C. Bambi, Constraints on the spacetime geometry around 10 stellar-mass black hole candidates from the disk's thermal spectrum, Astrophys. J. **797**, 78 (2014).
[129] M. Y. Piotrovich, Y. N. Gnedin, T. M. Natsvlishvili, and S. D. Buliga, Constraints on spin of a supermassive black hole in quasars with big blue bump, Astrophys. Space Sci. **362**, 231 (2017).
[130] R. Andrae, T. Schulze-Hartung, and P. Melchior, Do's and dont's of reduced chi-squared, arXiv:1012.3754.
[131] J. Nash and J. Sutcliffe, River flow forecasting through conceptual models part I—a discussion of principles, J. Hydrol. **10**, 282 (1970).
[132] D. R. Legates and G. J. McCabe, Evaluating the use of goodness-of-fit measures in hydrologic and hydroclimatic model validation, Water Resour. Res. **35**, 233 (1999).
[133] P. Krause, D. P. Boyle, and F. Bäse, Comparison of different efficiency criteria for hydrological model assessment, Adv. Geosci. **5**, 89 (2005).
[134] C. J. Willmott, On the evaluation of model performance in physical geography, in *Spatial Statistics and Models* (Springer, New York, 1984), pp. 443–460.
[135] C. J. Willmott, On the validation of models, Phys. Geogr. **2**, 184 (1981).
[136] I. Banerjee, S. Chakraborty, and S. SenGupta, Decoding signatures of extra dimensions and estimating spin of quasars from the continuum spectrum, Phys. Rev. D **100**, 044045 (2019).
[137] Z. Stuchlik and A. Kotrlova, Orbital resonances in discs around braneworld Kerr black holes, Gen. Relativ. Gravit. **41**, 1305 (2009).
[138] A. Chamblin, H. S. Reall, H.-a. Shinkai, and T. Shiromizu, Charged brane world black holes, Phys. Rev. D **63**, 064015 (2001).